Discovery of an Extreme MeV Blazar with the Swift Burst Alert Telescope

R.M. Sambruna, C. B. Markwardt, R.F. Mushotzky, J. Tueller, R. Hartman

NASA's GSFC, Greenbelt, MD 20771

W.N. Brandt, D.P. Schneider, A. Falcone, A. Cucchiara

Department of Astronomy & Astrophysics, The Pennsylvania State University, University

Park, PA 16802

M. F. Aller, H. D. Aller

University of Michigan, Ann Arbor, MI 48109-1042

I. Torniainen

Metsähovi Radio Observatory, Helsinki University of Technology, Metsähovintie 114,

FIN-02540 Kylmälä, Finland

F. Tavecchio, L. Maraschi

Osservatorio Astronomico di Brera, via Brera 28, 20121 Milano, Italy

M. Gliozzi

George Mason University, Dept. of Physics & Astronomy and School of Computational

Sciences, MS 3F3, 4400 University Drive, Fairfax, VA 22030

T. Takahashi

Institute of Space and Astronautical Science, 3-1-1 Yoshinodai, Sagamihara-shi, Kanagawa

229-8510, Japan

ABSTRACT

The Burst Alert Telescope (BAT) onboard *Swift* detected bright emission from 15–195 keV from the source SWIFT J0746.3+2548 (J0746 in the following), identified with the optically-faint (R $\sim$ 19), z=2.979 quasar SDSS J074625.87+244901.2. Here we present *Swift* and multiwavelength observations of this source. The X-ray emission from J0746 is variable on timescales of hours to weeks in 0.5–8 keV and of a few months in 15–195 keV, but there is no accompanying spectral variability in the 0.5–8 keV band. There is a suggestion that the BAT spectrum, initially very hard (photon index $\Gamma \sim 0.7$), steepened to $\Gamma \sim 1.3$ in a few months, together with a decrease of the 15–195 keV flux by a factor ~ 2. The 0.5–8 keV continuum is well described by a power law with $\Gamma \sim 1.3$, and spectral flattening below 1 keV. The latter can be described with a column density in excess of the Galactic value with intrinsic column density $N_H^z \sim 10^{22}$ cm^{-2}, or with a flatter power law, implying a sharp ($\Delta\Gamma \overset{>}{\sim} 1$) break across 16 keV in the quasar's rest-frame. The Spectral Energy Distribution of J0746 is double-humped, with the first component peaking at IR wavelengths and the second component at MeV energies. These properties suggest that J0746 is a a blazar with high gamma-ray luminosity and low peak energy (MeV) stretching the blazar sequence to an extreme.

Subject headings: Galaxies: active — galaxies: quasars: individual (J0746.3+2548)— X-rays: galaxies

1. Introduction

Among Active Galactic Nuclei (AGN), blazars are characterized by the most extreme properties, such as rapid variability, large apparent isotropic luminosity, high and variable polarization in the radio and optical, and emission across the entire electromagnetic spectrum, from radio wavelengths to GeV and TeV gamma-ray energies (e.g., Ulrich, Maraschi, & Urry 1997). These properties are ascribed to non-thermal (synchrotron and inverse Compton) emission from a relativistic jet seen nearly end-on. Blazars' Spectral Energy Distributions (SEDs) are double-humped in a power-per-decade representation, with the synchrotron component peaking anywhere from IR to X-rays, and the inverse Compton component extending up to gamma-rays. The SEDs form a sequence in luminosity, with more luminous sources having both peaks at lower energies than their fainter counterparts (Fossati et al. 1998, Ghisellini et al. 1998).

Traditionally, blazars have been selected at radio, optical, and X-ray wavelengths according to various criteria (e.g., Laurent-Mueheleisen et al. 1997, Perlman et al. 1998). Only a few sources were discovered using gamma-rays, both at GeV (Romani et al. 2004) and MeV wavelengths (Blom et al. 1995). The advent of detectors with improving sensitivity at hard X-ray energies (> 10 keV), is now providing a new window for blazar discovery and observation.

Such a window was recently opened by the Burst Alert Telescope (BAT; Barthelmy et al. 2005) onboard the *Swift* satellite. On December 15, 2004, the BAT began an ongoing monitoring of the sky with its wide-angle (2 steradians) field of view and high sensitivity in the 15–200 keV energy band. During the first 3 months of the sky survey operations, with a flux threshold of $\sim 10^{-11}$ erg cm^{-2} s^{-1}, the BAT detected several AGN, both radio-loud and radio-quiet (Markwardt et al. 2006). Here we describe the BAT discovery and subsequent *Swift* and multiwavelength observations of a new blazar with extreme

properties, SWIFT J0746.3+2548 (J0746 in the following). The source was identified with an optically-faint quasar at z=2.979 in the Sloan Digital Sky Survey (SDSS) archive. In this paper, we will present evidence that J0746 is a blazar (Flat Spectrum Radio Quasar) and more specifically, a new member of the MeV blazar class[1].

In Fall 2005, J0746 was the target of an X-ray (*Swift* and *Suzaku*), optical, and radio campaign. The radio observations were taken with the 26-m diameter U. of Michigan Radio Astronomy Observatory (UMRAO) and the 14-m diameter Metsähovi radio telescopes, while optical-UV photometry is from the *Swift* UVOT telescope. Here we present the *Swift* and radio observations, while a complete account of the *Suzaku* data will be forthcoming (Takahashi et al. 2006, in prep.). We also report on a new optical spectrum taken with the *Hobby-Eberly Telescope* (HET).

This paper is structured as follows. In § 2 we describe the source discovery and identification. The observations and data reduction procedures are presented in § 3, while in § 4 we give the results, in § 5 the discussion, and in § 6 the conclusions. We assume a concordance cosmology with $H_0 = 71$ km s^{-1} Mpc^{-1}, Ω_Λ=0.73, and Ω_m=0.27 (Spergel et al. 2003). The energy index α is defined such that $F_\nu \propto \nu^{-\alpha}$.

2. Discovery of J0746 at hard X-rays

During the first 3 months of its sky survey, the BAT discovered hard X-ray emission from several extragalactic sources (Markwardt et al. 2006). With a flux $F_{20-200\ keV} \sim 9 \times 10^{-11}$ erg cm^{-2} s^{-1} and a $> 7\sigma$ detection (Fig. 1), SWIFT J0746.3+2548 stands out as one of the brightest. The follow-up observations with the XRT in 0.5–10 keV shows the presence

---

[1]We define an MeV blazar as a blazar with peak of the Compton component in the SED at MeV energies.

of a source at RA(2000)= 07hrs 46m 25.6s, DEC(2000)=+25deg 49m 02.0s, or $1'$ from the BAT position. The radii of the error circles for the BAT and XRT positions are $2'$ and $3''$, respectively. No other X-ray sources are present in the XRT field of view, leading us to identify the XRT source with the origin of the BAT flux.

A comparison with the latest Sloan Digital Sky Survey (SDSS; York et al. 2000) Quasar Catalog (Schneider et al. 2005) yields a match with SDSS J074625.87+254902.2, located at RA(2000)=07h46m25.9, DEC(2000)=+25d49m02.1s; the accuracy of the SDSS coordinates is approximately $0.1''$. The SDSS counterpart of the X-ray source is an optically faint (R $\sim$ 19 mag) quasar at a redshift z=2.979. Using optical (Richards et al. 2006) and X-ray (Bauer et al. 2003) number counts, we estimate that the false-match probability of the XRT and SDSS sources is $P \sim 6.2 \times 10^{-6}$. Thus, the identification of the *Swift* source with SDSS J074625.87+254902.2 (J0746 in the following) is regarded as robust.

Because of its optical faintness, J0746 largely escaped the attention of the Astronomy community. A search of the NED database shows 23 references. Radio *VLBA* observations at 2.3 and 8.6 GHz show the quasar to be core-dominated, with no obvious extended radio features on mas scales (Fey & Charlot 2003). From the data in this paper, we calculate a radio-loudness parameter, $\log R_L \sim 3$, in the rest-frame of the quasar. The radio-loudness parameter is defined as the ratio of the 5 GHz to the V–band flux. To K-correct the radio and optical fluxes we used power law continua with $\alpha_{\nu,radio} = 0.08$ (see § 3.4) and $\alpha_{\nu,opt} = 0.54$ (§ 3.3).

Although J0746 was only recently identified as a quasar, the archival literature contains a number of observations of the object obtained during wide-angle surveys at a number of wavelengths. In the radio, J0746 was monitored at 8 and 2.3 GHz with the Green Bank Interferometer in the time period 1988–1995 (Lazio et al. 2001). No variability was detected at 2 GHz. However, the light curve at 8 GHz (32 GHz in the rest-frame) shows a slow but

smooth increase of the flux over 3 years, with a max/min flux change of a factor of 3. The radio spectral index steepens on the same timescale (Fig. 8 of Lazio et al. 2001).

The only previous X-ray observation of J0746 was by the *ROSAT* satellite during its All-Sky Survey (RASS). Weak 0.2–2 keV emission, with 16 counts in 438 sec, was recorded. Since the Galactic column density in the direction of J0746 is low, $N_H^{Gal} = 4.04 \times 10^{20}$ cm^{-2}, this implies a highly absorbed AGN; alternatively, *ROSAT* caught the quasar in a low intensity state.

Based on its broad-band properties, we argue in this paper in favor of a blazar nature of J0746 (§ 5).

3. Observations

3.1. X-rays

The *Swift* observations of J0746 are summarized in Table 1, where the BAT observations and follow-up XRT pointings are reported. The November 4 XRT observation was performed contemporaneously with *Suzaku* and radio measurements.

BAT: J0746 was in the BAT field of view for a total of 755 ks since the beginning of the survey on December 15, 2004. The results described here are for the first 9 months of the survey, or until the end of September, 2005. The average count rate from 15–195 keV is listed in Table 1.

The reduction of the BAT data was described in Marqwardt et al. (2005). Figure 1 shows the BAT significance map, ranging from -2σ (white) to $+8\sigma$ (black). Pixel size is 5′. The cross marks the SDSS position of J0746. The source is detected at $> 7\sigma$.

We extracted two BAT spectra, one for the initial 3.5 months of the survey, when J0746

was first discovered, and one integrated over the whole 9 months. The BAT spectrum of J0746 is based on the mosaicked sum of all observations which contain the source (mid Dec 2004 - mid Sep 2005). The minimum partial coding threshold was 15%. Before mosaicking, the images were corrected for systematic off-axis attenuation effects, such that the spectrum should remain relatively constant with off-axis angle (calibrated by BAT observations of the Crab).

The BAT spectra were fitted with XSPEC v.11.3.2, with the response matrix based on the latest (December 2005) calibration products. Because of the spectral extraction protocol, the BAT spectrum consists of 4 bins containing the source count rates in 4 energy bands: 14–25 keV, 25–50 keV, 50–100 keV, and 100–200 keV.

XRT: The XRT observed J0746 four times (Table 1). During the first three observations in September, which overlapped with the BAT observations (Fig. 2a), short exploratory exposures were used. On November 4, XRT observed J0746 for 15 ks, together with the UVOT, *Suzaku*, and ground-based radio observations. The XRT count rates in the four epochs are listed in Table 1.

We used the event2 files provided by the HEASARC, cleaned according to standard criteria (Capalbi et al. 2005). Only data acquired through Photon Counting (PC) mode, which has the maximum sensitivity, were used; no pileup is present at the source's count rates (Table 1). Light curves and spectra were extracted from a circular region centered on the XRT position and with radius $20''$. The background was extracted from a circle with radius $130''$ in a region free from obvious X-ray sources. Inspection of the background light curve shows no variability within the four XRT exposures.

The XRT spectra were rebinned in order to have at least 20 counts in the new bins, except for the first observation on 2005 September 5 (OBSID 002) where the spectrum was rebinned with a minimum of 10 counts/bin, to increase the number of data points at lower

energies (< 1 keV) for a meaningful determination of the column density. The spectra were fitted within XSPEC v.11.3.2 with the calibration files provided by the HEASARC, in the energy range 0.5–8 keV, where the calibration is best known and the background negligible.

3.2. Optical/UV photometry

UVOT: The *Swift* UVOT observed the source continuously (except for Earth occultations) starting at UT Nov 4 00:39 until UT Nov 6 15:59 (Table 2). During each orbit data were collected from the six filters, from the Optical to Ultraviolet wavelengths. Since the source is faint, we coadded all the data collected on the first day (Nov 4) in only one image for each filter. Similarly, the Nov 5 and Nov 6 data were coadded. The log of the UVOT observations, together with the fluxes, is given in Table 2.

The data analysis was performed using the uvotsource task included in the latest HEASOFT software release (http://swift.gsfc.nasa.gov/docs/software/lheasoft/). The background was subtracted, and corrections for coincidence loss effects (similar to pileup for the XRT) were applied. The magnitudes are converted into fluxes using the latest in-flight flux calibration factors and zero points. The source is well detected in the optical filters with over 3σ confidence level. There is no detection in the UV images, and only upper limits are reported in Table 2.

SDSS: Table 2 presents optical photometric measurements of J0746 obtained from the SDSS DR3 catalog in the SDSS system (Fukugita et al. 1996) on 19 December 2001. All fluxes are dereddened for Galactic absorption. The SDSS fluxes are consistent with those from the UVOT at similar wavelengths.

A search of the USNO archive for J0746 returns the following historical records of its optical flux: B=20.01, 19.87 mag; R=19.16, 19.04 mag; and I=18.92 mag. The B-band

measurements are consistent with those from the UVOT.

3.3. Optical spectra

SDSS: The SDSS spectrum of J0746 is displayed in the top panel of Figure 2. The data have a spectral resolution R $\sim$ 1900.

The optical spectrum of J0746 is that of a typical $z \approx 3$ quasar. Broad prominent emission lines, such as Lyα (4827 Å), C IV 1549 Å (6164 Å), and Si IV/O IV 1400 Å (5571 Å), typical of high-z quasars, are apparent in the spectrum. The continuum power law slope in the SDSS spectrum is $\alpha\nu \sim 0.54$, very near the canonical $\alpha\nu = 0.5$ from the SDSS quasar composite (Vanden Berk et al. 2001).

We calculated the observed EWs and fluxes of the detected lines. For C IV we find EW$_{obs}$=31 Å and F$_\lambda \sim 9.8 \times 10^{-16}$ erg cm^{-2} s^{-1}Å^{-1}, while for Si IV/O VI EW$_{obs}$=78 Å and F$_\lambda \sim 2.5 \times 10^{-15}$ erg cm^{-2} s^{-1}Å^{-1}, respectively. The EWs are within the distribution for radio-loud and radio-quiet quasars (Wills et al. 1993). There is no evidence for C IV absorption, either in the emission line or in the neighboring continuum.

HET: Blazars have notoriously variable levels of optical continuum which may dilute the emission lines during high states. We thus acquired a second optical spectrum of J0746 in 2005 Fall with the Hobby-Eberly Telescope (Ramsey et al. 1994). The HET spectrum of J0746 was obtained on 10 October 2005 with the Low Resolution Spectrograph (Hill et al. 1998). The 1.5″ slit, 300 line mm^{-1} grating, and GG385 filter produced a spectrum from 4000-8000 Å at a resolution R=460. The spectrum, which is the sum of two 900 s exposures, is shown in the lower panel of Figure 2.

The HET spectrum, taken 3.7 years (only 11 rest-frame months) after the SDSS one, shows very similar features. The HET continuum is redder and the lines slightly

stronger, but these changes should be considered marginal at best; the quality of the spectrophotometry of the SDSS data is considerably higher than that of the HET observation, and the change in the equivalent widths is not much more than 1σ. Thus, we can conclude that the level of the optical continuum did not significantly change between the epochs of the SDSS and HET observations.

3.4. Radio

The radio observations are presented in Table 3.

UMRAO: The University of Michigan radio data were obtained using the UMRAO 26-meter prime focus paraboloid antenna which is equipped with wide-band room temperature HEMPT (High Electron Mobility Pseudomorphic Transistor) amplifiers and operates at central frequencies of 4.8, 8.0, and 14.5 GHz. Measurements at all three of these frequencies utilize rotating, dual-horn polarimeter feed systems. An on-off observing technique was used at 4.8 GHz, and an on-on technique (switching the target source between the two feed horns closely spaced on the sky) was employed at 8 and 14.5 GHz. A typical observation consisted of a series of 8 to 16 individual measurements over a 25 to 45 minute period, depending on the observing frequency.

Observations of the program source were preceded and followed by observations of nearby calibrator sources (3C 144, 3C 145, 3C 218, 3C 274) selected from a grid across the sky; these calibration measurements were used to correct for temporal changes in the antenna aperture efficiency. Frequent drift scans are also made across stronger sources throughout every run to verify the telescope pointing correction curves. The flux scale for the UMRAO observations is set by observations of Cassiopeia A (e.g., see Baars et al. 1977). A more detailed explanation of the calibration and analysis techniques is given in

– 11 –

Aller et al. (1985). Interpolation of the radio fluxes in Table 3 yields a slope $\alpha_r = 0.08$, typical of a core-dominated source as shown by the *VLBA* images at 2.3 GHz and 8.5 GHz (Fey & Charlot 2003). Comparing our 8 GHz measurements with the long-term 8 GHz light curve in Fig. 8 of Lazio et al. (2001) shows that at the time of the *Swift* observations in November 2005 the source was in a high intensity state in the radio, similar to the maximum recorded in late 1992.

Metsähovi: Observations were also made with the 14-m diameter Metsähovi radio telescope at the frequency of 37 GHz. The fluxes are listed in Table 3.

The 37 GHz observations were made with the 13.7 m diameter Metsähovi radio telescope, which is a radome enclosed paraboloid antenna situated in Finland (24 23' 38"E, +60 13' 05"). The measurements were with a 1 GHz-band dual-beam receiver centered at 36.8 GHz. The HEMPT front end operates at room temperature. The observations are ON–ON observations, alternating the source and the sky in each feed horn. A typical integration time to obtain one flux density data point is 1200–1400 s.

The flux density scale is set by observations of DR 21. Sources 3C 84 and 3C 274 are used as secondary calibrators. A detailed description of the data reduction and analysis is given in Teräsranta et al. (1998). The error estimate in the flux density includes the contribution from the measurement rms and the uncertainty of the absolute calibration.

4. X-ray results

4.1. Timing analysis

Here we discuss the results of a timing analysis of the XRT and BAT data. Variability was assessed through the use of a χ^2 test, with related probability P_{χ^2} that the light curve is constant; thus, small values of P_{χ^2} indicate significant variability.

BAT: The BAT light curve in the energy range 15–195 keV is shown in Figure 3a. Bins are 15-day averages. The vertical ticks mark the dates of the three September XRT observations. The BAT light curve is formally consistent with a constant, with $P_{\chi^2}=0.12$.

XRT: The XRT light curves were extracted in soft (0.5–2 keV), hard (2–8 keV), and total (0.5–8 keV) energy bands. We searched for spectral changes by computing hardness ratios defined as the ratio of the hard and soft X-ray light curves.

Figure 3b shows the XRT long-term light curve from 0.5–8 keV, obtained from the average count rates at the four observing epochs in Table 1. From Figure 3b it is apparent that the flux changed by a factor $\gtrsim 2$ on timescales of a week. The χ^2 test confirms variability, with $P_{\chi^2} < 10^{-5}$. No spectral changes were observed, with the plot of the hardness ratios versus time being constant ($P_{\chi^2} \sim 0.098$).

Next, we searched for variability within the XRT individual exposures. Figure 4 shows the 0.5–8 keV light curves at the four epochs, rebinned at 2000 sec resolution. Flux variations are observed at every epoch, and most notably during the Sept 5 and Nov 4 observations. A χ^2 test for these two light curves yields significant variability, with $P_{\chi^2} < 10^{-3}$ and $P_{\chi^2} \sim 9 \times 10^{-5}$, respectively. At the beginning of the Sept 5 observation the flux increases by a factor 2.5 in one hour, albeit within large uncertainties. A similar increase of the flux on a timescale of ~ 2 hrs is also present at the beginning of the Nov 4 observation. On this date, more modest variations are also seen throughout the exposure, on similar timescales (1–2 ks). No significant spectral variability is detected in either the Sept 5 or Nov 4 data, as shown by the the hardness ratio light curve ($P_{\chi^2} > 0.06$).

We also investigated the energy-dependence of the variability by calculating the variability amplitude relative to the mean count rate, F_{var}, corrected for effects of random errors (e.g., Edelson et al. 2002), for both hard and soft Nov 4 light curves. In practice, however, due the paucity of data points and the large statistical errors, only in few cases

were we able to estimate F_{var}. There is a suggestion of a larger variability amplitude at harder X-rays, with $F_{var,hard}$=0.160 and $F_{var,soft}$=0.05 for the hard, although higher quality data are necessary to reach firmer conclusions.

Comparison to previous X-ray observations: As mentioned above, J0746 was detected during the RASS with a 0.2–2 keV count rate of 0.04 c/s. To compare the *ROSAT* and *Swift* observations, we converted the RASS 0.2–2 keV count rate into an XRT 0.5–8 keV count rate. Using `PIMMS` and assuming an absorbed power law with column density $N_H = 3 \times 10^{21}$ cm^{-2} and photon index $\Gamma = 1.3$ (see below), we find that the 0.5–8 keV count rate at the time of the RASS observation was 0.041 c/s, comparable to the lower state of the XRT observation in September 3 (Table 1). Thus, at the time of the *ROSAT* sky survey J0746 was in a lower X-ray intensity state.

We conclude that the medium-hard X-ray emission of J0746 is variable. There is a hint for larger-amplitude variations at the harder energies, which will be tested in the *Suzaku* observation.

4.2. Spectral analysis

4.2.1. The X-ray continuum

The results of the spectral fits to the XRT and BAT spectra are reported in Table 4. The best-fit parameters and their 90% uncertainties for one parameter of interest ($\Delta\chi^2$=2.7) are listed, together with the observed fluxes and intrinsic (absorption-corrected) luminosities.

BAT: We fitted the BAT spectra with a single power law model without an absorption column density, as the hard X-rays are not affected by the relatively small column densities measured with the XRT (see below). The BAT continuum from the first 3.5 months of the

survey, when the source was discovered, is fitted by a very hard power law, $\Gamma \sim 0.74$. The isotropic X-ray luminosity of $L_{15-150~keV} \sim 9 \times 10^{47}$ erg s^{-1} makes J0746 one of the most luminous extragalactic sources at hard X-rays to-date.

The BAT continuum from the whole 9 months integration, however, is described by a steeper power law, $\Gamma = 1.3$. The derived flux is a factor 2 lower than from the 3-months spectrum, implying that the source was already fading after the first 3 months. However, as shown in the top panel of Figure 5, this is only a $\gtrsim 1\sigma$ effect. The high-energy spectral variability properties of J0746 will be better quantified in the *Suzaku* HXD observations.

XRT: The XRT spectra were initially fitted with a single power law with the Galactic column density. At all epochs, the residuals of this model showed a deficit of flux below 3 keV, indicating the presence of spectral flattening at these energies. This is illustrated in the bottom panel of Figure 5, where the residuals of a power law with Galactic N_H from the joint fits to the 4 epochs is plotted. The flattening below 3 keV can be interpreted as due either to excess absorption over Galactic, or as a flatter power law component. We tested both possibilities by fitting the XRT data with two models: 1) a single power law plus an additional free column density, N_H^z, at the source rest-frame; and 2) a broken power law with Galactic absorption only.

For model 1, the choice of an intrinsic absorber is motivated by the fact that no evidence for absorption due to an intervening medium is present in the optical spectra of the quasar (Fig. 2). Moreover, excess X-ray absorption along the line of sight was previously found to be common in $z > 1$ radio-loud quasars (see Worsley et al. 2006 and references therein), but not in coeval radio-quiet sources, suggesting the absorbing medium is located near the central engine of the AGN (Elvis et al. 1992, Fiore et al. 1998, Page et al. 2005).

The fit with model 1 is reported in Table 4. In the three longest observations (obsids 002, 003, 007), the addition of the intrinsic absorber is significant at 99% confidence

($\Delta\chi^2$=5) for 002 and 003, and at 92% ($\Delta\chi^2$=4) confidence for 007, according to the F-test. The measured intrinsic column density is $N_H^z = (1 - 4) \times 10^{22}$ cm^{-2}, and the photon index is $\Gamma = 1.3$, at the flat end of the distribution for $z > 1$ radio-loud quasars with $\log R_L \approx 3$ (Page et al. 2005). In the case of obsid 001, corresponding to the lowest intensity state and shortest exposure time, the column density and slope from a free-fit are poorly constrained; we thus repeated the fit by fixing N_H^z to the average value from the fits to the remaining three observations. This yields $\Gamma \sim 1.3$, similar to the other three exposures and confirming that the 0.5–8 keV flux changes with no accompanying spectral variations (within 20%).

Extrapolating the best-fit model of the November XRT observation to energies $>$ 10 keV yields a $F_{15-150\ keV} = 2.4 \times 10^{-11}$ erg cm^{-2} s^{-1}. This is a factor 4 smaller than the flux from the 9-months survey, when the BAT flux was already declining. It is thus likely that during the November 2005 campaign the source was in a low state.

Acceptable fits were obtained from model 2, a broken power law with Galactic absorption; the parameters are reported in Table 4. Indeed, in the case of the longest exposure of November, the broken power law model is formally preferred (at 98% confidence, $\Delta\chi^2$=8) to model 1. This is a well-known observed phenomenon in high-z radio-loud quasars: the spectral flattening at soft energies can be equally well described by a power law with absorption (either cold or warm) and a convex broken power law. We will revisit this issue in § 5.3.

We thus conclude that the XRT spectra are well-described by a single power law with strong spectral flattening below a few keV, which can be described in terms of excess absorption over the Galactic value (Table 4). Acceptable fits are also obtained with a convex broken power law, yielding $\Delta\Gamma \sim 1.1$ at 4 keV.

4.2.2.   Limits on the Fe Kα emission line

Usually, in blazars the beamed jet emission dilutes or overwhelms the reflection features from the disk, yielding a featureless X-ray spectrum (Sambruna, Chou, & Urry 2000). However, during a low state of the non-thermal emission the Fe Kα line can be detected. For example, in 3C 273, Grandi & Palumbo (2004) observed a variable EW of the Fe Kα line and estimated that the X-ray disk spectrum is diluted by the beamed radiation of the jet by a factor 1.2 to 2.8 from 2–10 keV, while the jet always dominates above 40 keV. Similarly, a Fe Kα line with EW $\sim$ 100 eV was detected from the cores of two powerful quasars hosting one-sided *Chandra* jets (Sambruna et al. 2006, in prep.).

We thus investigated the presence of an Fe Kα emission line in J0746, which in this source is redshifted to 1.61 keV, at the peak of the detector effective area. We concentrated on the Nov 4 spectrum, which has the best signal-to-noise ratio. An unresolved (width $\sigma_l = 0.05$ keV) Gaussian line with rest-frame energy fixed at 6.4 keV was added to the power law best-fit model. The 90% confidence upper limit to the rest-frame EW is 200 eV.

No evidence for such a line is present in the other datasets. Adding a Gaussian line at 1.61 keV to the power law model that best-fits the four datasets jointly yields $\Delta\chi^2 = -1$, indicating that the Gaussian component is not needed.

5.   Discussion

5.1.   What is J0746?

Below we discuss the evidence supporting the classification of J0746 as a high luminosity blazar, or more precisely a Flat Spectrum Radio Quasar (FSRQ), due to its prominent broad emission lines in the optical. The high energy emission however can only

be attributed to a relativistic jet.

5.1.1. Multiwavelength Variability

One of the defining properties of blazars is their variability, often dramatic, at all observed wavelengths from radio to gamma-rays (Ulrich et al. 1995). Indeed, in J0746 flux and spectral variability is observed in the radio and X-rays, the two bands with the best coverage so far.

J0746 was observed as part of the Green Bank Interferometry monitoring program at 2.3 and 8 GHz during the years 1979-1996 (Lazio et al. 2001). Correlated flux and spectral variability was observed at 8 GHz, with a flux increase by a factor 3 in 3 years and steeper slope with increasing flux. This is similar to other FSRQs in the Lazio et al. sample.

In the optical-UV, the *Swift* UVOT measurements are consistent with the magnitudes from the SDSS, and with historical records (§ 3.3). While this needs to be confirmed by future monitoring, the lack of variability in this band is consistent with the idea that the optical/UV radiation comes from a different component, most likely the thermal emission from the disk. A straightforward test could be provided by polarimetry, with a highly polarized optical flux arguing against a thermal origin and in favor of a non-thermal one.

J0746 was detected by the BAT at > 10 keV with a bright flux. This is similar to other blazars. Bright ($\sim 10^{-10}$ erg cm^{-2} s^{-1}) emission was detected with the BAT (Giommi et al. 2006, submitted) and *INTEGRAL* (Pian et al. 2006) from the $z{=}0.859$ FSRQ 3C 454.3, while a rapid (lasting 2 ks) flare was detected with *INTEGRAL* in 20–40 keV at the position of the $z{=}0.902$ blazar NRAO 530 (Foschini et al. 2006). Thus, it is reasonable to expect significant shorter-term flux variability at energies > 10 keV from J0746 in future more sensitive observations.

The X-ray variability is better constrained in the 0.5–8 keV energy band. The XRT light curves of J0746 show flux changes of a factor 2 on timescales of hours to weeks and months. There is a hint that the hard X-rays vary with larger amplitude than the softer energies, but this finding needs to be confirmed by future observations. However, while the 0.5–8 keV flux varies, there are no accompanying spectral variations. This is similar to other FSRQs at lower z observed with $ASCA$ and $ROSAT$ (Donato et al. 2001; Sambruna 1997), and to other radio-loud quasars at $z > 1$ (Page et al. 2005).

The large X-ray luminosity and rapid variability of J0746 provide further support for the idea that its emission is beamed. In fact, assuming the X-ray emission from J0746 is isotropic, we can derive a limit to the radiative efficiency η. Following Fabian (1979), $\eta > 4.8 \times 10^{-43} \Delta L / \Delta t$ erg s^{-1} s^{-1}, where ΔL is the luminosity change in a time interval Δt (Brandt et al. 1999). From Table 4 and Figure 4d, $\Delta L \sim 5 \times 10^{46}$ erg s^{-1} and $\Delta t \sim 1800$ sec in the quasar's rest-frame. Thus, $\eta > 13$, which is unphysically large unless we require relativistic beaming of the radiation.

5.1.2.   Broad-band spectral indices

The broad-band energy distributions of blazars can be described to first approximation with the spectral indices α_{ro}, α_{ox}, and α_{rx}. These are defined as the two-point indices between radio (5 GHz) and optical (V band), optical and X-rays (1 keV), and radio to X-rays. Based on the radio-to-X-ray flux ratio, blazars can be further classified as High-Energy Peaked BL Lacs (HBLs), with $\alpha_{rx} < 0.8$; and Low-energy Peaked BL Lacs (LBLs) and FSRQs, with $\alpha_{rx} > 0.8$ (Padovani & Giommi 1995).

When plotted in the $\alpha_{ro} - \alpha_{ox}$ plane, blazar classes occupy distinct, although partly overlapping, regions. For HBLs, $\alpha_{ro} < 0.6$ and $\alpha_{ox} < 1.3$, while LBLs and FSRQs have

$\alpha_{ro} > 0.5$ and $\alpha_{ox} > 1.0$ (e.g., Donato et al. 2001). Using rest-frame flux densities at 5 GHz, in V band, and at 1 keV, the broad-band spectral indices of J0746 are $\alpha_{rx} = 0.78, \alpha_{ro} = 0.65$, and $\alpha_{ox} = 1.03$. Thus, J0746 appears to be a borderline source between FSRQs and HBLs.

It is useful to compare the broad-band indices of J0746 to radio-quiet quasars, because this could indicate the level of boosting of the continuum due to beaming. A recent extensive compilation of broad-band indices for radio-quiet quasars is provided by Strateva et al. (2005). Here, they define an optical-to-X-ray index as the slope between the flux at 2 keV and at 2500 Å in the quasar's rest-frame. For J0746, this index is 1.16, much flatter than the radio-quiet quasars in Strateva et al. (2005). Thus, for a given optical flux, the X-ray emission from J0746 is more than a factor 10 larger than expected for radio-quiet quasars. This also suggests that, at least to a first approximation, beaming affects the X-ray emission of J0746 but not (or much less) its optical-UV flux.

5.1.3. The Spectral Energy Distribution (SED)

As discussed in § 1, a strong spectral signature of blazars is the presence of a double-peaked structure in their SEDs. Similarly, as shown in Figure 6, J0746 exhibits a double-humped SED.

To assemble the SED of J0746, we used data from this paper as well as from the literature. In Figure 6 the radio (filled circles), optical, UV, and X-ray (XRT, 0.5–8 keV) fluxes are contemporaneous measurements from our November 4 campaign, while the filled triangles are archival observations from NED. Also plotted is the 9-months BAT spectrum (see below). As such, the SED in Figure 6 contains contemporaneous (radio, optical, UV, and medium-hard X-rays) data as well as archival fluxes.

At GeV energies, we plot an upper limit to the EGRET flux from a reanalysis of four

archival images. Unfortunately, the coverage of the J0746 field by EGRET was very poor: EGRET observed the source in 1992, 1993, 1994, and 1995. However, J0746 was never closer than 16.7° to the EGRET axis; this implies that no high-quality exposure of the source was ever acquired. The upper limit to the > 100 MeV flux from the combined four observations is 5×10^{-8} ph cm^{-2} s^{-1} and is plotted in Figure 6 with an arrow.

The first striking feature in Figure 6 is that, as implied by the hard BAT spectrum and the EGRET limit, the peak of the second spectral component is located around a few MeV. This would make J0746 a new member of the poorly known MeV blazars subclass, which so far contains only two sources detected by COMPTEL (Blom et al. 1996; for PKS 0208–512 see, however, Stacy et al. 2003). The obvious caveat is, of course, that the BAT and EGRET fluxes are not simultaneous, while FSRQs notoriously vary at high energies on timescales of days.

The second important feature in Figure 6 is the steep optical-to-UV continuum, which implies a peak of the synchrotron component at IR wavelengths. Observations of J0746 in the near and far-IR are urged to better sample the SED in this critical portion of the spectrum. It is tempting to interpret the steep optical-UV emission as the high-energy tail of thermal emission from the accretion disk, i.e., the so-called blue bump, usually observed in quasars (Elvis et al. 1994) but also in a few FSRQs (3C 273; von Montigny et al. 1997).

In conclusion, based on multiwavelength evidence, we classify J0746 with a high-z blazar. Further observations, especially polarimetry at radio through optical wavelengths, are strongly encouraged to confirm the blazar nature of this source.

Below we model the SED of J0746 in the assumption that J0746 is a blazar, and that the optical-to-UV continuum at the time of the UVOT observations is due to thermal emission from the disk.

5.2. Modeling the Spectral Energy Distribution

The continuum from blazars is generally attributed to synchrotron and inverse-Compton (IC) emission (e.g., Ghisellini et al. 1998; for a different view see Atoyan & Dermer 2003 and references therein) produced within a jet pointing toward the observer. In the case of blazars showing strong emission lines, as in J0746, the target photons for the IC process are likely dominated by those belonging to the external radiation field (disk, broad line region), amplified by relativistic effects in the plasma rest-frame (Dermer & Schlickeiser 1993, Sikora et al. 1994). Synchrotron self-Compton emission (Maraschi et al. 1992), on the other hand, can substantally contribute in the soft X-ray band (e.g., Ballo et al. 2002).

Again, we caution that the SED in Figure 6 contains non-simultaneous data. In particular, the BAT and XRT spectra were taken several months apart, while the BAT spectrum was integrated over a long-time period (9 months). The choice to use the 9-months BAT spectrum in the SED modeling is due to the fact that it is "closer" in time to the Nov 4 campaign data; indeed, the extremely flat continuum during the initial higher state, $\alpha \sim -0.26$, posits severe problems for current blazar models.

To reproduce the observed SED we have applied the synchrotron-IC emission model fully described in Maraschi & Tavecchio (2003). Briefly, the emission region is modeled as a sphere with radius R, in motion with bulk Lorentz factor Γ at an angle θ with respect to the line of sight, and filled with tangled magnetic field (with intensity B) and relativistic electrons. Γ and θ are combined in the Doppler factor $\delta = [\Gamma(1 - \beta\cos\theta)]^{-1}$, where $\beta = v/c$. The (purely phenomenological) electron distribution is modeled as a smoothed broken power law, with indices n_1 and n_2 below and above the break Lorentz factor γ_b. The electron distribution extends within the limits $\gamma_{\min} < \gamma < \gamma_{\max}$.

The exceptionally steep optical-UV continuum strongly suggests that the emission in this band is dominated by a thermal-like component, possibly associated with the

blue-bump component which characterizes the quasar optical region (e.g., Sun & Malkan 1989), usually thought to be associated with the putative accretion disk. This interpretation is justified by the presence of prominent emission lines in the HET spectrum of J0746 (§ 3.2), which was taken a few weeks after the end of the BAT observations discussed here.

The identification of the optical-UV component with the disk emission constrains the disk luminosity $L_D \sim$ a few $\times 10^{47}$ erg s^{-1}. We choose to model this component with a black body peaking at the typical frequency of 10^{15} Hz (in the quasar rest-frame). The external radiation field is modelled as the same black-body, diluted within the broad line region, supposed to be spherical with radius R_{BLR}. This radiation approximates the radiation reprocessed and re-isotropized by the BLR clouds. Its luminosity is fixed to a fraction τ of the luminosity L_D of the putative central illuminating disk.

The resulting model is reported in Figure 6 (solid line), with the parameters listed in the caption. From the inferred parameters and assuming the composition of one proton per emitting electron (for the reason of this choice see Maraschi & Tavecchio 2003), we can infer a kinetic power of the jet of $P_j = 4 \times 10^{48}$ erg s^{-1}. This can be compared with the radiative output of the disk $L_{\mathrm{D}} = 4 \times 10^{47}$ erg s^{-1}. The ratio $P_j/L_D \sim 10$ is of the same order of what is found in other cases for which both powers can be estimated with reasonable accuracy (Tavecchio et al. 2000; Maraschi & Tavecchio 2003). The parameters used to reproduce the SED are close to those usually found for other powerful blazars (e.g., Maraschi & Tavecchio 2003, Ghisellini et al. 1998).

An interesting aspect of the *Swift* results is the exceptionally flat spectrum measured in the hard X-rays. Flat spectra ($\alpha_X = 0.3$) characterize several high-luminosity blazars (e.g., Tavecchio et al. 2000). To model such hard spectra we use an electron index of $n_1 = 1.5$. Such a flat electron distribution poses serious problems for the standard scenarios usually discussed, involving shock acceleration or cooling processes, which lead to a typical

distribution with $n = 2$. An interesting possibility has been considered by Sikora et al. (2002). They assume a two-step acceleration process: the flat portion is produced by a pre-acceleration mechanism (e.g., stochastic acceleration driven by turbulence or reconnection), while the steep portion after the peak is produced through the standard shock acceleration.

In the radio band, our data fits well to a power law spectrum with $\alpha = 0.48$, quite typical of a transparent synchrotron source. Without a high resolution VLBI image, the most straight forward interpretation is that there is an extended region around the central core that is responsible for the radio-mm flux. The IR-optical emission is presumably produced in a core region that starts appearing at shorter wavelengths, but without data in the sub-mm it is not possible to specify exactly where the BLR region starts to dominate. The discontinuity between the radio-mm spectrum and the shorter wavelength emission is consistent with a high energy cutoff in the radiating particles in this extended emitting region; such a cutoff is already part of the model parameters used to fit the core region at shorter wavelengths.

It is worth noting that we fix γ_{min} to 1. Larger values would in fact produce an unobserved deficit of soft X-ray photons, further flattening the X-ray spectrum. This is also typical of this kind of sources, and seems to support the two-step view, in which the bulk of the electrons remains at low energies.

Finally, while we have assumed that the steep optical-UV continuum in Figure 6 is thermal in origin and related to the accretion disk, we can not exclude *a priori* that the jet does not contribute to a fraction of the optical flux, or even dominates it during outbursts. In this sense, variability of the optical-UV continuum in J0746 would have to be modeled as a mix of a non-thermal, variable jet component and a thermal, less variable one related to the accretion.

5.3.   J0746 in context

There is evidence that the double-humped SEDs of blazars form a continuous sequence in luminosity (Sambruna, Maraschi, & Urry 1996). In this sequence, going from the more luminous FSRQs to the fainter and closer TeV BL Lacs, the synchrotron component peak shifts from IR to X-ray wavelengths, while the Compton peak shifts, by the same amount, from GeV to TeV gamma-rays (Fossati et al. 1998). Models of the SED sequence suggest that particle energies decrease and magnetic fields increase with increasing luminosities while the Doppler factor is approximately constant (Ghisellini et al. 1998). The sequence finds a physical basis in the run of the jet and disk powers, P_{jet} and P_{disk}, with $P_{jet} \sim P_{disk} \sim 10^{46} - 10^{47}$ erg s^{-1} for FSRQs and $P_{jet} > P_{disk}$ for BL Lacs (Tavecchio et al. 2000; Maraschi & Tavecchio 2003).

To compare the SED of J0746 to other blazars, we have plotted in Figure 7 the blazar luminosity sequence from the reanalysis of Donato et al. (2001). The solid line represents the best-fit model to the SED of J0746 from Figure 6. It is apparent that the spectral properties of this source are extreme in the blazar class: as discussed above, the synchrotron peak likely lies below the IR frequency range while the IC peak is at MeV energies. This qualifies J0746 as a member of the poorly known "MeV blazars" subclass (Blom et al. 1996).

There is much debate whether the blazar sequence is intrinsically true or a product of several observational biases, especially at gamma-rays (Urry 1999), or limited sensitivity of current radio and optical surveys (Nieppola, Tornikoski, & Valtaoja 2006; Anton et al. 2004). Nevertheless, here we used the sequence as a comparison template to showcase the unusual properties of J0746. Note that, if the sequence is true, the SED of J0746 would be extreme, but not unexpected.

A property J0746 shares with other high-z radio-loud quasars is the presence of spectral

hardening in the X-ray spectrum below a few keV. As discussed in § 4.2.1, this can be modeled in terms of either excess absorption along the line of sight, or a flatter power law. We now discuss the two scenarios in turn.

In the context of blazar emission models, a continuum break at soft X-rays can be expected if the particle distributions responsible for the high-energy component have a low-energy cutoff, parameterized by the value of the minimum Lorentz factor of the relativistic electrons (Tavecchio et al. 2000). In this scenario, the hardening occurs below $\sim \gamma_{min}^2 \Gamma^2 \nu_{ext}$, with $\nu_{ext} \sim 10^{15}$ Hz (Fig. 6). The fitted value of the break energy in J0746 would thus imply $\gamma_{min} \sim 3$, consistent with the SED modeling (Fig. 6).

Alternatively, the spectral flattening below 3 keV can be described in terms of excess N_H along the line of sight, as originally advocated for high-z radio-loud quasars by Elvis et al. (1992). Recent *XMM-Newton* observations have confirmed that at least a fraction of these sources could have intrinsic absorption, with $N_H^z \sim 10^{22} - 10^{23}$ cm^{-2} (see Worsley et al. 2006 and references therein). The nature and location of the absorber, however, is still debated today. The large X-ray column densities would imply large optical reddening for the quasars, which is not seen.

Such difficulty exists for J0746 as well. The SDSS and HET spectra indeed show little or no intrinsic reddening, at odds with the X-ray column density $N_H \sim 10^{22}$ cm^{-2} which implies $A_V \sim 10$ (assuming Galactic dust-to-gas ratios). Moreover, while several X-ray absorbed quasars, both radio-loud and radio-quiet, show accompanying UV absorption lines (e.g., Brandt, Laor, & Wills 2000), this is not the case for J0746 (Fig. 2). This would seem to indicate a dust-free, neutral absorber. However, perhaps the major difficulty is to devise a physically plausible location for the absorber. As shown in Figure 6 the X-ray emission from J0746 comes from a highly beamed ($\delta \sim 20$) jet, at least in its inner regions. One can thus speculate that the absorbing medium is located inside the jet, perhaps ambient

gas entangled in the moving blobs (e.g., Celotti et al. 1998). However, whether this gas has a covering factor large enough to produce significant spectral depression in the X-ray continuum (Fig. 5) remains to be proven.

In conclusion, the nature of the low-energy spectral flattening in J0746 is still an open question. We look forward to the deeper (100 ks), broad-band *Suzaku* spectrum which will hopefully settle the issue.

6. Summary and Conclusions

The BAT experiment onboard *Swift* detected bright emission in the energy range 15–150 keV from the radio-loud quasar J0746 at z=2.979, implying an isotropic luminosity around $\sim 10^{48}$ erg s^{-1}. Rapid variability in 0.5–10 keV strongly suggests beaming. In this paper, we reported the *Swift* discovery observations and follow-up multiwavelength monitoring of this source. The main results are:

- The X-ray emission of J0746 is variable on timescales of days to months (Fig. 3, 4). Fast variability on timescales of 1–2 ks is observed for the 0.5–8 keV flux (Fig. 3b).

  At all epochs, the XRT hardness ratio light curve is consistent with a constant value, implying there is no spectral variability on short (hours) timescales in 0.5–8 keV.

- The 15–150 keV emission is consistent with a very hard continuum, $\Gamma \sim 0.74$, during the first 3 months of the BAT survey, and a steeper continuum, $\Gamma \sim 1.3$, with halved flux, in the BAT spectrum integrated over 9-months.

- The 0.5–8 keV spectrum is well described by a $\Gamma \sim 1.3$ power law. Spectral flattening is present at < 1 keV, which can be interpreted as excess absorption over the Galactic value, implying an intrinsic column density $N_H^z \sim 10^{22}$ cm^{-2}, or a flatter power law

component, implying a sharp ($\Delta\Gamma \sim 1.1$) spectral break around 16 keV in the quasar's rest-frame.

- The Spectral Energy Distribution of J0746 has a double-humped structure, with the first component peaking around IR wavelengths and the second component likely at a few MeV. The luminosity of the source is dominated by the high-energy emission.

Based on the results presented in this paper, we conclude that J0746 is a blazar, and more precisely, a Flat Spectrum Radio Quasar. Its SED has extreme, but not unexpected, properties compared to other blazars. Additional and possibly simultaneous multiwavelength observations of J0746 are encouraged to confirm the jet-origin of its emission; to this end, polarization measurements at radio and optical wavelengths will be especially revealing.

The detection of a flare at high-energies from J0746 raises several outstanding questions. How common are sources like J0746? What are the physical parameters of MeV blazar jets? What causes the violent outbursts at hard X-rays, and what is their duty cycle? The latter issue is particularly important in view of the possibility that blazars are significant, and even dominant, contributors to the gamma-ray sky (Salamon & Stecker 1994). The BAT flux variability on timescales of months, as well as the BAT detection of several other sources with properties similar to J0746 (Sambruna et al., in prep.), suggests that flares at energies > 10 keV may be common from these blazars, stressing the key importance of wide-angle, sensitive and continuous sky monitoring at these energies.

REFERENCES

Aller, H. D., Aller, M. F., Latimer, G. E., & Hodge, P. 1985, ApJS, 59, 513

Anton, S., Browne, I. W. A., March, M. J. M., Bondi, M., & Polatidis, A. 2004, MNRAS, 352, 673

Atoyan, A. M., & Dermer, C. D. 2003, ApJ, 586, 79

Baars, J. W. M., Genzel, R., Pauliny-Toth, I. I. K., & Witzel, A. 1977, A&A, 61, 99

Ballo, L., et al. 2002, ApJ, 567, 50

Barthelmy, S.D. et al. 2005, Space Science Rev., in press (astroph/0507410)

Bauer, F. et al. 2004, AJ, 128, 2048

Blom, J.J. et al. 1996, A&AS, 120, 107

Brandt, W.N., Laor, A., Wills, B.J. 2000, ApJ, 528, 637

Brandt, W.N., Boller, Th, Fabian, A.C. & Ruszkowski, M. 1999, MNRAS, 303, L53

Capalbi, M., Perri, M., Saijia, B., Tamburelli, F., & Angelini, L. 2005, "The SWIFT XRT Data Reduction Guide", version 1.2

Cappi, M. et al. 1997, ApJ, 478, 492

Celotti, A., Kuncic, Z., Rees, M. J., & Wardle, J. F. C. 1998, MNRAS, 293, 288

Dermer, C.D. & Schlickeiser, R. 1993, ApJ, 416, 458

Donato, D., Ghisellini, G., Tagliaferri, G., & Fossati, G. 2001, A&A, 735, 739

Edelson, R., Turner, T. J., Pounds, K., Vaughan, S., Markowitz, A., Marshall, H., Dobbie, P., & Warwick, R. 2002, ApJ, 568, 61

Elvis, M. et al. 1994, ApJS, 95, 1

Elvis, M., Fiore, F., Wilkes, B., McDowell, J., & Bechtold, J. 1992, ApJ, 422, 60

Fabian, A.C. 1979, Proc. R. Soc. London, Ser. A., 366, 449

Fabian, A.C. et al. 2001, MNRAS, 323, 373

Fiore, F., Elvis, M., Giommi, P., & Padovani, P. 1998, ApJ, 492, 79

Foschini, L. et al. 2006, A&A, in press (astroph/0601101)

Fossati, G., Maraschi, L., Celotti, A., Comastri, A., & Ghisellini, G. 1998, MNRAS, 299, 433

Fukugita, M., Ichikawa, T., Gunn, J.E., Doi, M., Shimasaku, K., & Schneider, D.P. 1996, AJ, 111, 1748

Ghisellini, G. et al. 1998, MNRAS, 301, 451

Giommi, P. et al. 2006, A&A, submitted

Grandi, P. & Palumbo, G.C. 2004, Science, 306, 998

Hill, G.J., Nicklas, H.E., MacQueen, P.J., Mitsch, W., Wellem, W., Altmann, W., Wesley, G.L., & Ray, F.B. 1998, Proc. SPIE, 3355, 433

Laurent-Muehleisen, S. A., Kollgaard, R. I., Ryan, P. J., Feigelson, E. D., Brinkmann, W., & Siebert, J. 1997, A&AS, 122, 235

Lazio, T.J.W., Waltman, E. B., Ghigo, F. D., Fiedler, R. L., Foster, R. S., & Johnston, K. J. 2001, ApJS, 136, 265

Maraschi, L., & Tavecchio, F. 2003, ApJ, 593, 667

Maraschi, L., Ghisellini, G., & Celotti, A. 1992, ApJ, 397, L5

Markwardt, C. et al. 2006, ApJ, in press

Nieppola, E., Tornikoski, M., & Valtaoja, E. 2006, A&A, 445, 441

Page, K. L., Reeves, J. N., O'Brien, P. T., & Turner, M. J. L. 2005, MNRAS, 364, 195

Perlman, E.S., Padovani, P., Giommi, P., Sambruna, R.M., Jones, L. R., Tzioumis, A., & Reynolds, J. 1998, AJ, 115, 1253

Pian, E. et al. 2006, A&A, in press (astroph/0602268)

Ramsey, L.W., Sebring, T.A., & Sneden, C. 1994, Proc. SPIE, 2199, 31

Richards, G.T. et al. 2006, AJ, subm. (astro-ph/0601434)

Romani, R. W., Sowards-Emmerd, D., Greenhill, L., & Michelson, P. 2004, ApJ, 610, L9

Salamon, M.H. & Stecker, F.W. 1994, ApJ, 430, L21

Sambruna, R.M. 1997, ApJ, 487, 536

Sambruna, R.M., Maraschi, L., & Urry, C.M. 1996, ApJ, 463, 444

Schneider, D.P., et al. 2005, AJ, 130, 367

Sikora, M., Błażejowski, M., Moderski, R., & Madejski, G. M. 2002, ApJ, 577, 78

Spergel, D.N. et al. 2003, ApJS, 148, 175

Stacy, J.G., Vestrand, W.T., & Sreekumar, P.G. 2003, ApJ, 598, 216

Strateva, I.V., Brandt, W. N., Schneider, D. P., Vanden Berk, D. G., & Vignali, C. 2005, AJ, 130, 387

Sun, W.-H., & Malkan, M. A. 1989, ApJ, 346, 68

Tavecchio, F., et al. 2000, ApJ, 543, 535

Tersranta, H., Tornikoski, M., Mujunen, A. et al. 1998, A&AS, 132, 305

Teräsranta et al. (1998), A&A, 132, 305

Ulrich, M.-H., Maraschi, L., & Urry, C.M. 1997, ARA&A, 35, 445

Urry, C.M. 1999, Astroparticle Physics, Vol. 11, Nos. 1–2, p. 159

Vanden Berk, D.E., et al. 2001, AJ, 122, 549

von Montigny, C. et al. 1997, ApJ, 483, 161

Wills, B.J., Brotherton, M. S., Fang, D., Steidel, C.C., & Sargent, W.L.W. 1993, ApJ, 415, 563

Worsley, M.A., Fabian, A.C., Pooley, G.G., & Chandler, C.J. 2006, MNRAS, in press (astroph/0602355)

York, D.G., Adelman, J., Anderson, J.E., Anderson, S.F., et al. 2000, AJ, 120, 1579

Table 1: X-ray Observations

Instrument	Obs ID	Date	Start Time	End Time	Exposure	Count rate
(1)	(2)	(3)	(4)	(5)	(6)	(7)
BAT	$\cdots$	survey	12/04/04	09/30/05	755,000	$(6.2 \pm 7.2)\times 10^{-4}$
XRT	00035200001	Sept 3	07:17:36	12:14:59	1928	0.0456 ± 0.006
	00035200002	Sept 5	04:13:33	09:15:58	2712	0.0667 ± 0.005
	00035200003	Sept 9	01:29:31	22:33:58	3210	0.0879 ± 0.005
	00035200007	Nov 4	00:39:56	23:29:58	15,356	0.0613 ± 0.002

Explanation of Columns: 1=Detector name; 2=Observation ID; 3=Date of observation in 2005, except for the BAT where the data are from the 9-months survey; 4=Start time (UT); 5=End time (UT); 6=Exposure time in sec; 7=Background-subtracted count rate in 15-150 keV for BAT and in 0.5–8 keV for the XRT.

Table 2: Optical Observations

Filter	Wavelength	Date	Mag	Flux	Exposure
(1)	(2)	(3)	(4)	(5)	(6)

Swift UVOT

Filter	Wavelength	Date	Mag	Flux	Exposure
V	5460	MJD 53678	18.95 ± 0.19	92.7 ± 16.2	1382
B	4350		19.91 ± 0.17	48.2 ± 0.8	915
U	3450		19.88 ± 0.17	17.8 ± 0.3	1235
W1	2600		> 20.32	> 8.8	2572
M2	2200		> 21.49	> 3.2	4028
W2	1930		> 21.41	> 3.4	5584
V	5460	MJD 53679	19.35 ± 0.16	64.1 ± 0.9	2123
B	4350		19.42 ± 0.12	75.6 ± 0.8	1217
U	3450		19.97 ± 0.17	16.4 ± 0.3	2123
W1	2600		> 21.63	> 2.6	4251
M2	2200		> 22.22	> 1.6	6978
W2	1930		> 22.64	> 1.1	8491

SDSS

Filter	Wavelength	Date	Mag	Flux	Exposure
u	3571	Dec 19, 2001	20.76	18.0	
g	4653		19.71	47.4	
r	6147		19.50	57.5	
i	7461		19.42	61.9	
z	8904		19.48	58.6	

Explanation of Columns: 1=Filter; 2=Center wavelength in Å; 3=Date of observation; 4=Observed magnitude; 5=Derived flux in μJy, dereddened for Galactic absorption; 6=Exposure in sec.

Table 3: Radio Observations

Date	Freq.	Flux	Unc.
(1)	(2)	(3)	(4)

UMRAO			
09/25	8.0	0.52	0.02
10/07	8.0	0.79	0.07
10/08	8.0	0.65	0.01
10/20	14.5	0.49	0.06
11/04	8.0	0.68	0.03
11/05	8.0	0.66	0.05
11/08	4.8	0.82	0.02
11/10	4.8	0.81	0.03
11/11	4.8	0.86	0.02
11/12	8.0	0.64	0.03

Metsähovi			
11/02	37	0.36	0.09
11/02	37	0.44	0.06
11/02	37	0.49	0.08
11/04	37	0.48	0.11
11/04	37	0.58	0.08

Explanation of Columns: 1=Date (MM/DD) of 2005; 2=Frequency in GHz; 3=Flux density in Jy; 4=Uncertainty on the flux density.

Table 4: Spectral Fitting Results

Obs.	N_H^z	Γ	χ^2/dofs	Flux	Lum
(1)	(2)	(3)	(4)	(5)	(6)
BAT					
3 months	$\cdots$	$0.74^{+0.29}_{-0.72}$	0.33/2	142	135
9 months	$\cdots$	$1.34^{+0.40}_{-0.39}$	0.18/2	79.9	189
XRT[a]					
00035200001	40^{+81}_{-38}	$2.37^{+1.63}_{-1.24}$	1.32/3	2.2	32
	3.4 fix	$1.25^{+0.41}_{-0.33}$	1.56/4	2.6	7.2
00035200002	$4.2^{+4.7}_{-3.2}$	$1.30^{+0.27}_{-0.25}$	1.20/17	4.1	12.1
00035200003	$4.7^{+4.1}_{-2.9}$	$1.38^{+0.26}_{-0.22}$	0.72/11	4.8	16.7
00035200007	$1.4^{+1.5}_{-1.1}$	1.31 ± 0.11	1.3/43	3.1	9.7
	4.04 fix	$\Gamma_1^b = 1.04^{+0.11}_{-0.17}$	1.15/42	2.8	8.0
		$\Gamma_2^c = 2.14^{+1.17}_{-0.66}$			

Explanation of Columns: 1=Observation ID (see Table1); 2=Column density in 10^{22} cm^{-2} at the redhsift of the source; 3=Photon index; 4=Reduced χ^2 and degrees of freedom (dofs); 5=Observed 20–200 keV (BAT) and 2–10 keV (XRT) flux in 10^{-12} erg cm^{-2} s^{-1}; 6=Intrinsic (absorption-corrected) 20–200 keV (BAT) and 2–10 keV (XRT) luminosity in 10^{46} erg s^{-1}.

Notes: a=A column density fixed to the Galactic value (4.04×10^{20} cm^{-2}) was included in all the fits. b=Photon index below the break energy $E_b = 4.0^{+0.9}_{-2.5}$ keV from a fit with a broken power law model; c=Photon index above the break energy $E_b = 4.0^{+0.9}_{-2.5}$ keV from a fit with a broken power law model.
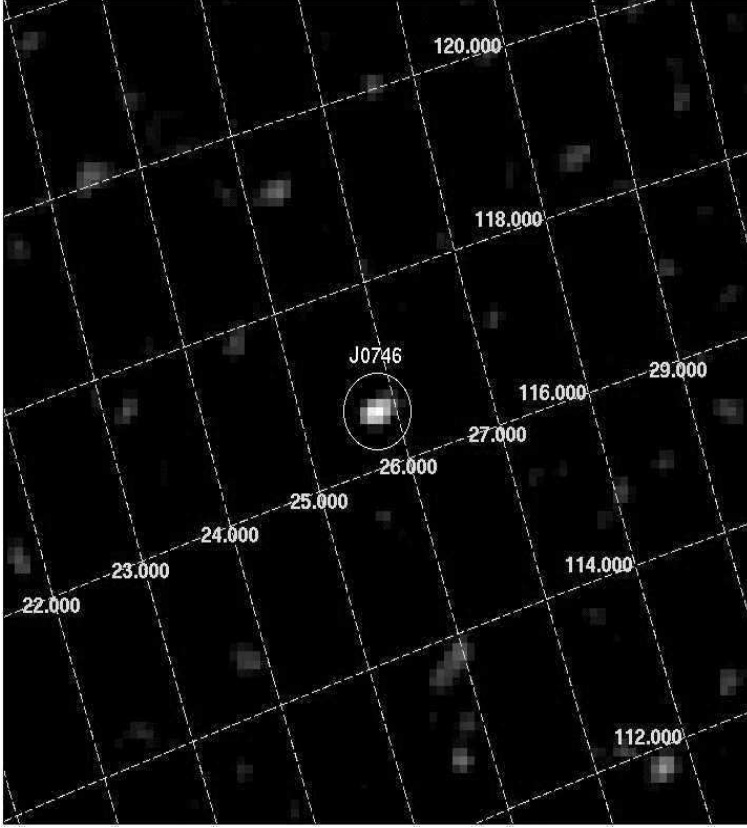
Fig. 1.— The BAT sensitivity image of J0746, ranging from 2σ (white) to 7.5σ (black) for a total exposure time of 755 ks. The image is 10°x 10°, with $5'$ pixels. The circle marks the position of J0746. The orientation is arbitrary. J0746 is detected at 7.5σ.
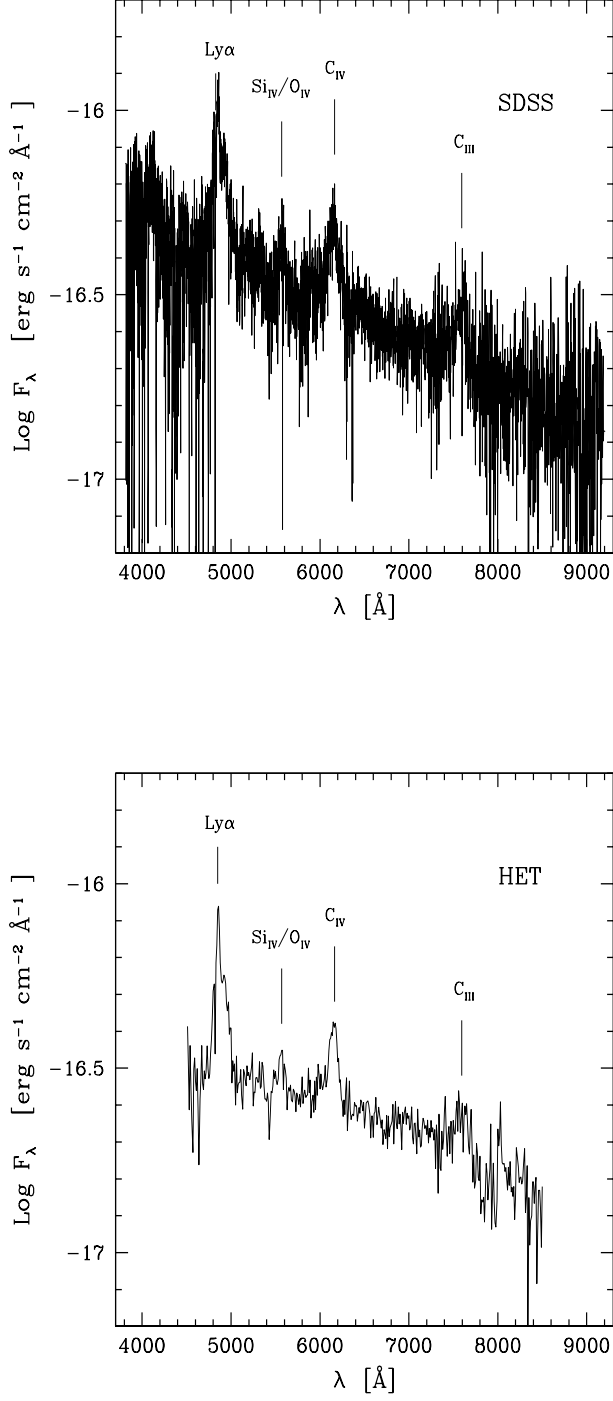
Fig. 2.— The SDSS (**Top**) and HET (**Bottom**) spectra of J0746, showing typical broad UV lines of a high-redshift quasar. The SDSS spectrum was taken December 19, 2001 and has a resolution R=1900; the HET spectrum, taken on October 10, 2005, has a resolution R=460.
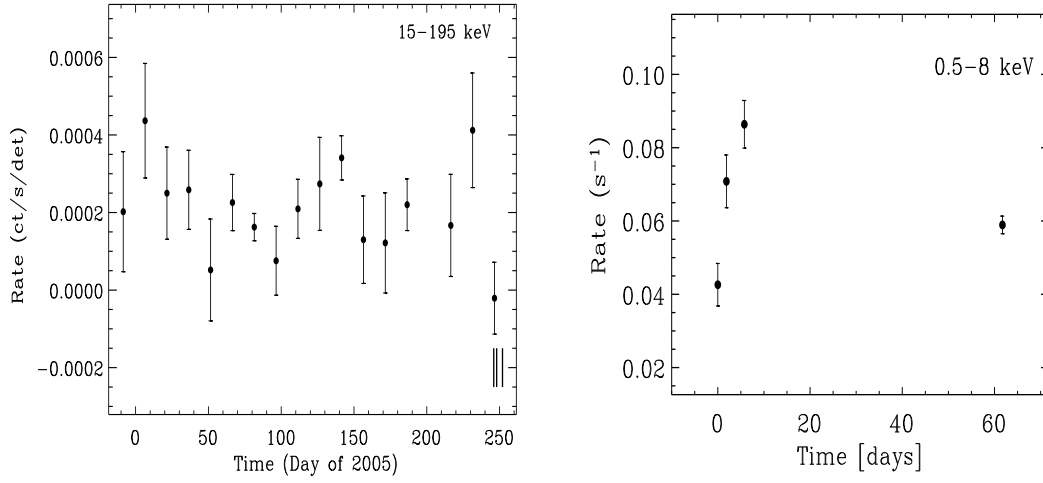
Fig. 3.— **(a, Left):** The BAT light curve of J0746 from 15–195 keV. Bins are 15-day averages. The start date is December 15, 2004. The vertical bars in September mark the times of the follow-up XRT observations (Table 1). **(b, Right):** The *Swift* XRT light curve, obtained by averaging the count rate for each observing epoch (Table 1). Variation of the 0.5–8 keV flux of a factor $\gtrsim 2$ in 5 days are apparent.
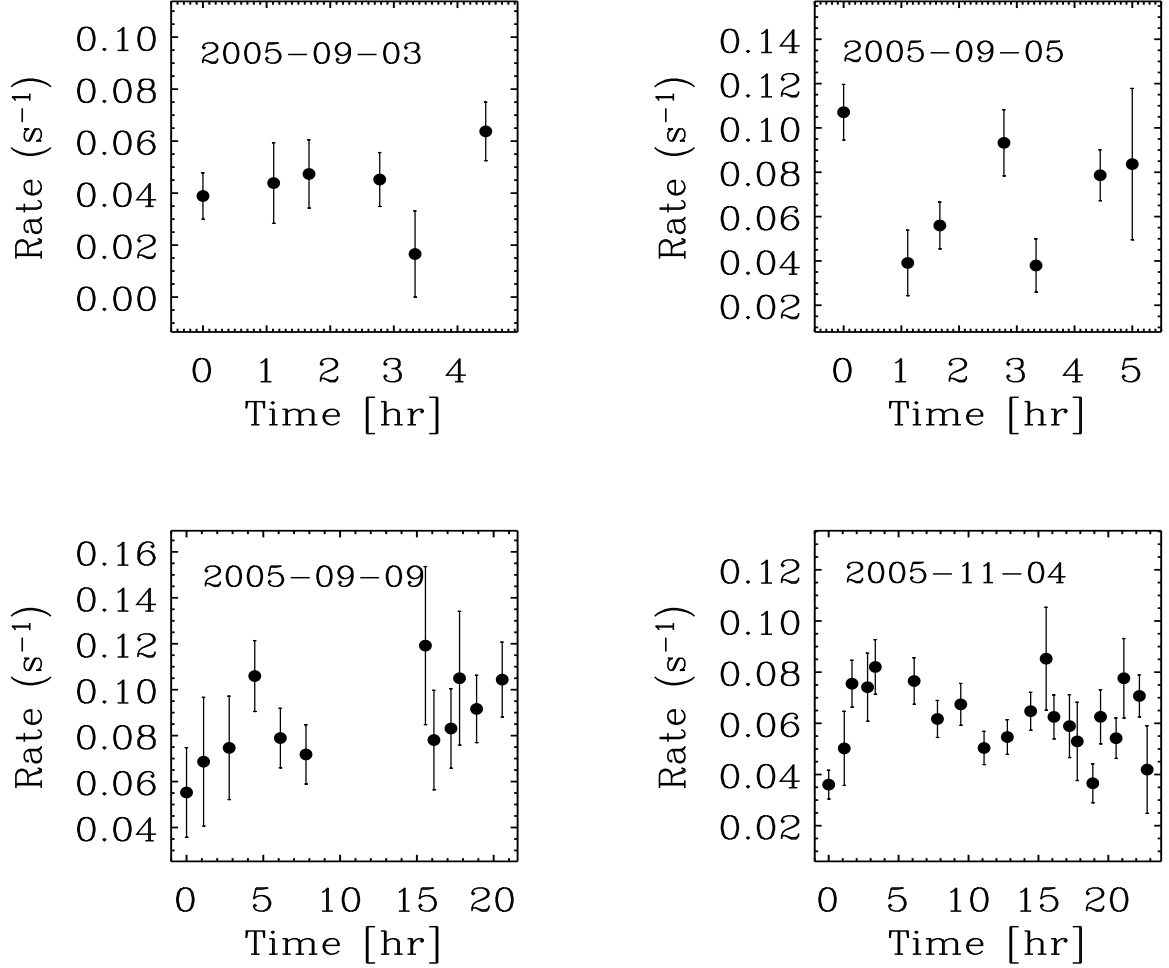
Fig. 4.— The *Swift* XRT light curves in total band (0.5–8 keV) at the four epochs. Significant flux variability is present in the Nov 4 and Sept 5 observations. The flux changed by a factor 2.5 in one hour in September and by a factor $\gtrsim 2$ in 10 days in November. There is no accompanying spectral variability as indicated by the hardness ratio light curve which is consistent with a constant (see text).
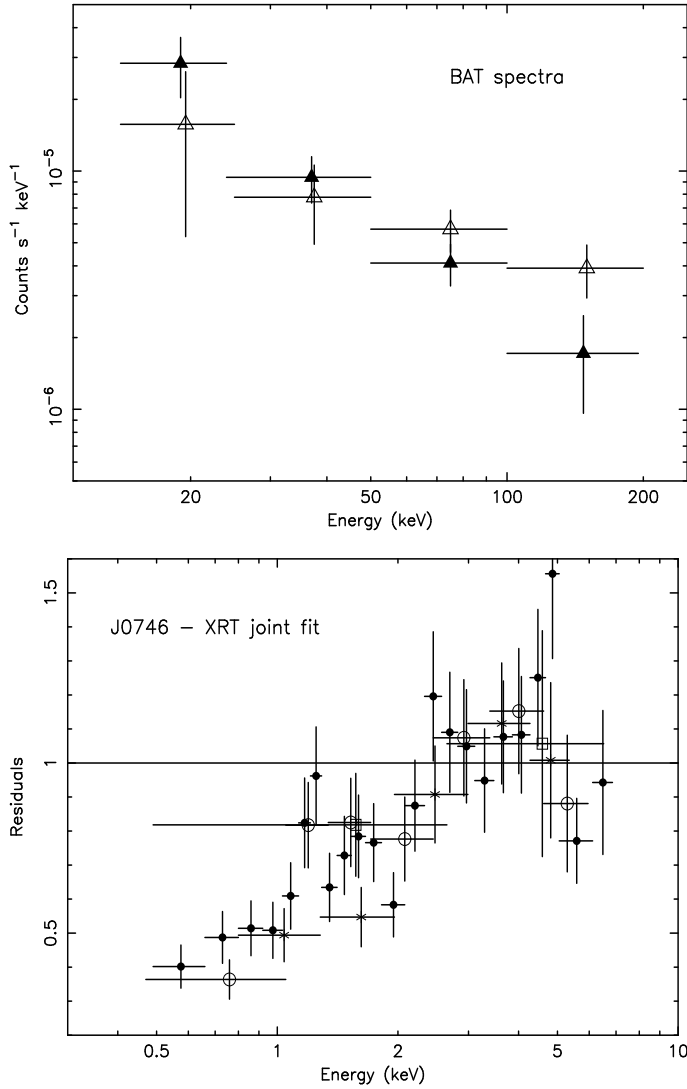
Fig. 5.— **Top:** The BAT spectra from the 3 months *(open triangles)* and 9 months *(filled triangles)* integrations. There is a suggestion for the 3-months spectrum to be harder, albeit at only $\gtrsim 1\sigma$. **Bottom:** Residuals of a joint fit to the XRT spectra of J0746 with a power law and Galactic absorption only. The data from the four epochs of observations were fitted simultaneously in the energy range 2–8 keV, with the lower-energy datapoints added back. This plot clearly illustrates the spectral flattening below 3 keV at all epochs. *Open squares:* obsid 001; *Asterisks:* obsid 002; *Open circles:* obsid 003; *Filled squares:* obsid 007.
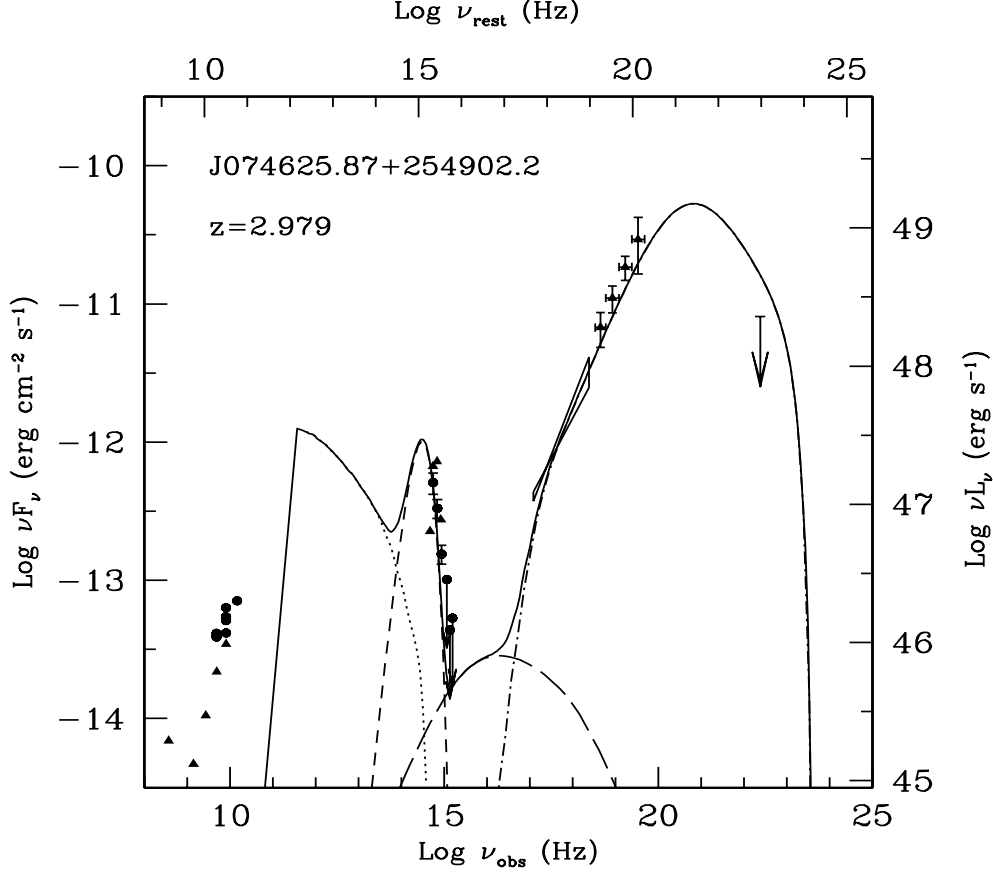
Fig. 6.— Spectral Energy Distribution of J0746 from archival and coeval observations. The BAT spectrum from the 9 months exposure is plotted, together with the XRT spectrum, UVOT, and radio (filled circles) fluxes from the November 4 campaign. The data plotted with triangles are from NED, while the GeV upper limit is from our reanalysis of the EGRET database. The SED is fitted with a composite jet+disk model. The solid line shows the jet continuum calculated with the emission model described in the text, assuming the following parameters: $\Gamma = \delta = 20$, $R = 2.7 \times 10^{16}$ cm, $B = 2$ G, electron density $n_e = 9 \times 10^4$ cm^{-3}, $\gamma_{\min} = 1$, $\gamma_{rmb} = 50$, $\gamma_{\max} = 10^3$, $n_1 = 1.5$, $n_2 = 3.8$. The external radiation field has a luminosity $L_{\mathrm{BLR}} = 10^{46}$ erg/s and is diluted within the BLR assumed to have a radius $R_{BLR} = 10^{18}$ cm. The single emission components are also reportes: synchrotron (dotted), SSC (long dashed), EC (dot-dash) and the disk (dashed). The peak of the synchrotron component is produced by the self-absorption.
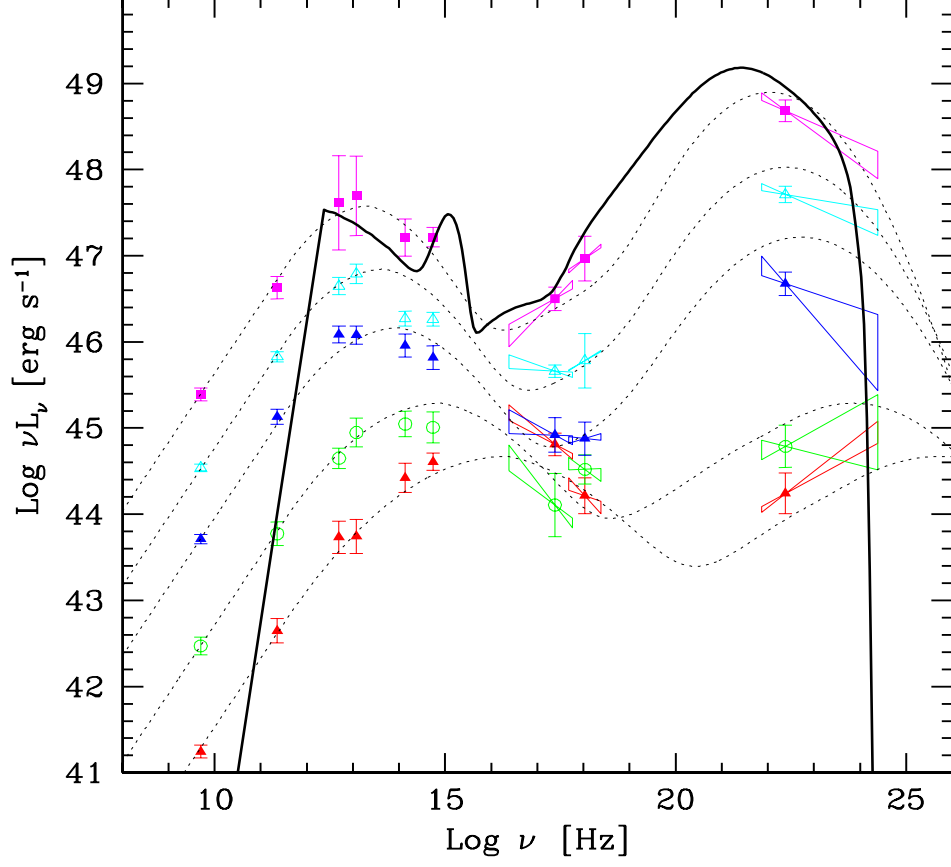
Fig. 7.— The Spectral Energy Distributions (SEDs) of blazars form a sequence with luminosity (Fossati et al. 1998). Going from luminous FSRQs to fainter TeV BL Lacs, the synchrotron and IC peaks move forward, and the Compton flux decreases. The solid black line is the best-fit model to the SED of J0746, showcasing its extreme properties.